SPATIAL DISTRIBUTION OF DUST FROM CIRRUS TO DENSE CORES

A. Abergel[1], P. André[3], A. Bacmann[3], J.-P. Bernard[1], S. Bontemps[2], F. Boulanger[1], A. Coulais[1], F.X. Désert[5], E. Falgarone[4], A. A. Kaas[2], M. Huldtgren[2], M.A. Miville-Deschênes[1], L. Nordh[2], G. Olofsson[2], M. Pérault[4], & J.-L. Puget[1]

[1]Institut d'Astronomie Spatiale, 91405 Orsay Cedex, France
[2]Stockholm Observatory, S-133 36 Saltsjöbaden, Sweden
[3]Service d'Astrophysique, Centre d'Etudes de Saclay, 91191 Gif-Sur-Yvette Cedex, France
[4]Radioastronomie Millimétrique, Ecole Normale Supérieure, 24 rue Lhomond,75005 Paris, France
[5]Observatoire de Grenoble, BP 53, 414 rue de la piscine, 38041 Grenoble Cedex 9 France

ABSTRACT

Large scale mapping of several star forming regions in the interstellar medium has been conducted with ISOCAM in two broad-band filters (5-8.5 and 12-18 μm). The small scale (3-6 arcsec) extended mid-IR emission of dust at different stages of evolution and in a wide range of illuminations and densities has been revealed.
The structure of the infra-red emission of illuminated edges of nearby molecular clouds gives strong constraints on the penetration of UV radiations through these clouds and on their small scale density structure. For both the Horsehead nebula and the interface of the main cloud of ρ Ophiuchi, the edges of the molecular clouds strongly illuminated by B stars present extremely steep increases of column density, while the extinction of incident radiation inside the clouds appears compatible with homogeneous matter at small scale (typically below $\sim$ 0.01 pc).
Dense cores are seen as deep absorption structures against a diffuse background emission. The density profiles derived from the extinction profiles depart from a r^{-2} law due to a central flattening (typically for r < 0.02 pc). The steepest gradients in outer regions can be modelled with density profiles at least as steep as a r^{-2} law.
Finally ISOCAM data also allow to extend the statistical analysis of the spatial distribution of dust in the diffuse interstellar medium down to a few arcsec scales.

Key words: Interstellar medium, dust, extinction, density structure, PDR, dense cores

1. INTRODUCTION

Before ISO, the IRAS observations have given a complete view of the dust in our galaxy with an angular resolution of 4', within broad-band filters at 12, 25, 60 and 100 μm. The spectral coverage has been extended from the stellar scattered light (below 5 μm) to the millimeter emission by the the Far Infrared Absolute Spectrophotometer (FIRAS) and the Diffuse Infrared Background Experiment (DIRBE) on board of COBE, with a low angular resolution (7° and 40 arcmin respectively). The far IR emission together with the UV/visible interstellar extinction can be in the general case explained by three different components of interstellar particles (Désert et al. 1990, Dwek et al. 1997): (1) Large grains (of size $\geq$ 10 nm) in thermal equilibrium with the radiation field contribute to most of the sub-mm emission (T$\sim$17-20 K in cirrus clouds), (2) Large aromatic molecules explain the mid-IR emission features (Léger et al. 1989) and (3) Very Small Grains (VSGs) have a size intermediate between large grains and large molecules (Sellgren et al. 1985). Both large aromatic molecules and VSGs are transiently heated at high temperature each time they absorb a UV photon. They cool off radiating in the near and mid-infrared.
Images of the dust emission allow to study the spatial structure of clouds, the interaction of young stars with nearby dense gas, the propagation of radiation and more generally the evolution of dust within the interstellar medium. IRAS data have revealed IR emission everywhere in the galaxy, with a spectacular auto-similarity on a very wide range of scales and densities. An important result is also the variations of the colors of the IR emission (e.g. Boulanger et al. 1990) which imply local changes in the relative abundance of the different dust particles.
However IRAS was not able to spatially resolve individual structures, because of the limited angular resolution ($\sim$ 4'). In the interstellar medium, features as small as $\sim$1 arcsec (for nearby complexes: $\sim$200 AU or 10^{-3} pc) are detected with interferometric molecular observations (Falgarone et al. 1998), and structures of a few 10 AUs are revealed by absorption measurements (Diamond 1989, Marscher et al. 1993). Ground-based observations in the mid-IR can only be performed within limited spectral range and at high resolutions for very bright objects (for instance M17, Giard et al. 1994).
Part of the ISO guaranteed time program, the ISOCAM survey of nearby star forming regions has been conducted with the two broad-band filters LW2 and LW3 (5-8.5 and 12-18 μm, respectively) with an an-

Proceedings of the Conference "The Universe as seen by ISO", Paris, France, 20–23 October 1998 (ESA SP-427, March 1999)

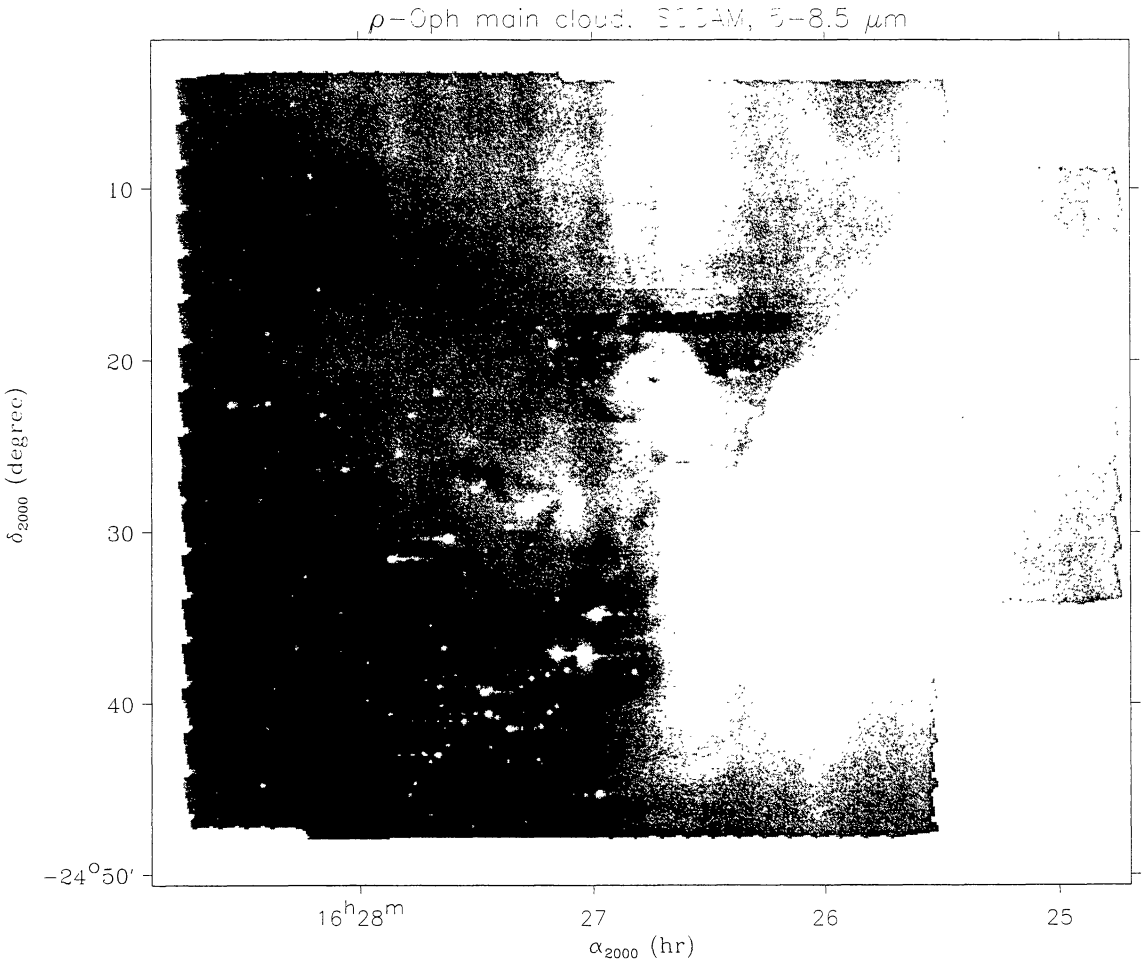

Figure 1. ISOCAM map of the ρ Ophiuchi main cloud with the LW2 filter (5-8.5 μm).

gular resolution of 3-6 arcsec. ISOCAM, SWS and ISOPHOT data have confirmed that, from cirrus to bright reflection nebulae, most of the emission within these two filters is due to emission features characteristic of C-C and C-H bonds in aromatic hydrocarbons (Boulanger et al. 1997, Mattila et al. 1996, Moutou et al. 1997). The intensity of these features globally scales with the UV radiation field (Boulanger et al. 1997). A continuum underlying the features, due to the same emitters and/or VSGs, may also contribute to the intensity measured within the two filters.
The observation strategy and the list of targets of the survey have been described by Olofsson et al. (1998). ISOCAM has an angular resolution and sensitivity of (Cesarsky et al. 1996) which greatly increases our ability to describe the small structure of the Interstellar Medium (e.g., Abergel et al. 1996). After discussing the actual status of the data reduction, we present some recent results.

2. DATA REDUCTION

Data were taken with the Long-Wavelengths (LW) channel of ISOCAM. The data reduction is made through a pipeline which filters all unpredictable events (essentially impacts of cosmic ray particles and long-term drifts), and inverts a model of the response (dark, transient effects, photometry). The accuracy of the processed data strongly depends (1) of the efficiency of the methods used to filter unpredictable events, and (2) on the accuracy of the model of the response.
Cosmic ray particles have continuously hit the detector. In the general case, the response of the affected pixels instantaneously increases (which produces a "glitch"), then recovers after one or two readouts. These events are discarded using a temporal median filtering which detect all pixels deviating from the running median value by more than a threshold value. Typically a few % of the data are affected. Impacts due to heavy ions are significantly less fre-

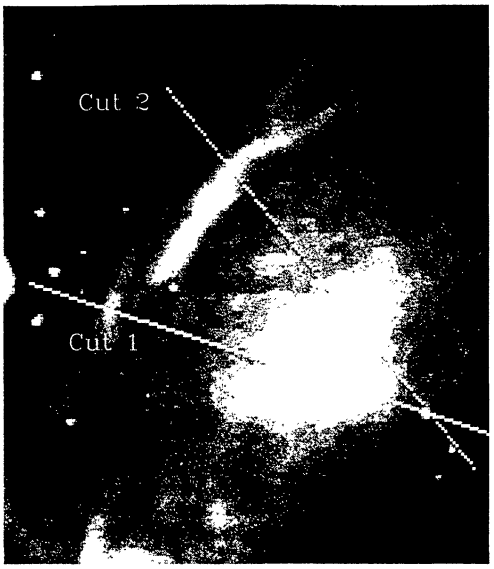

Figure 2. Bright filaments along the illuminated interface of ρ Ophiuchi main cloud (with the LW2 filter). The star HD147889 is at the intersection of the two slices (corresponding to cuts 1 and 2 of Fig. 3).

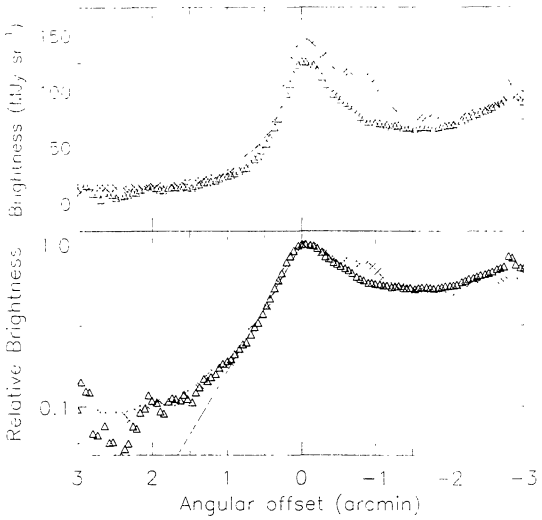

Figure 3. Upper panel: Brightness profiles (for the LW2 filter) along the two slices of Fig. 2 (Crosses: cut 1, Triangles: cut 2). Bottom panel: The same in relative and logarithmic scales. The solid line corresponds to the extinction law $I(z) = I_0\ e^{-Kz}$, with $K = 1.8\ arcmin^{-1}$.

quent, but produce glitches with significant memory effects (Désert et al. 1998). At the present time, they are not removed in the data of this survey, since actually no method allows to remove them systematically. However the time constant is large (typically more than several minutes) and part of the effects can be removed by applying a flat-field correction variable with the time (see below).

For each readout is subtracted a dark image computed using the estimator of the time behaviour of the dark signal (Biviano 1998). The detector presents systematic memory effects of the response which can bias the photometry by a factor of typically 40% (Abergel et al. 1999). The data of the survey have been processed two years ago using a simple empirical model (Abergel et al. 1996), with a final photometric accuracy of ∼10%. A new approach based on an analytical inversion of a physical model (Coulais & Abergel these proceedings) gives, for uniform illumination, an accuracy quite better (∼1%). We are currently testing this method for our images which generally contain strong gradients of illumination (point sources,...). Paradoxically, the signal to noise ratio is actually NOT better for strong sources than for faint sources because of the not proper correction of the transient response.

One flat-field image was extracted from each raster by computing the mean value of the lowest percentile (20%) seen by each pixel, excluding frames with strong emission above the zodiacal background. However large scale gradients of the sky brightness may contaminate this image. Therefore we use an iterative process to improve the flat-field correction and include a temporal dependence (Miville-Deschênes et al. 1999). Finally coadded images are projected on the sky map. A very long-term transient affects may affect typically 5-10% of the flux above the dark level during several hours. This effect, critical to study the large scale variations of brightness with low amplitude, is still not fully characterised (we do not know whether it is reproducible or not). Spectacular results are obtained using the redundancy of the observations, by comparing in an iterative process the flux measured for pieces of sky which has been observed at different times during the observations (Miville-Deschênes et al. 1999). In any case and at the present time, the data reduction to analyse the extended emission in the data of the survey is not yet definitive. Finally we remove the zodiacal emission at the time of the observations using the model of Reach et al. (1995) calibrated from the DIRBE/COBE data.

3. ILLUMINATED INTERFACES

3.1. The PDR of the ρ Ophiuchi main cloud

The ρ Ophiuchi main cloud L1688 is one of the nearest star forming complex (∼ 160 pc, Bertiau 1958). It contains a large number of Young Stellar Objects (YSOs) identified by ISOCAM (Bontemps et al. these proceedings) and previous surveys. The unusually high IR brightness is due to large column densities (A_v up to 100) combined with the presence of early type stars and YSOs. We have already shown (Abergel et al. 1996) that small scales spatial structures are mainly due to dust locally heated by embedded B stars, while large scale emission is due to external heating. The map discussed in Abergel et al. 1996 has been extended to the West (Figure 1) and now contains the B2V star HD147889 which illuminates the western interface. The star appears included in an empty cavity since it does not illuminate any dust located in its surrounding. A large fraction of the emission to the West of the map is due to dust

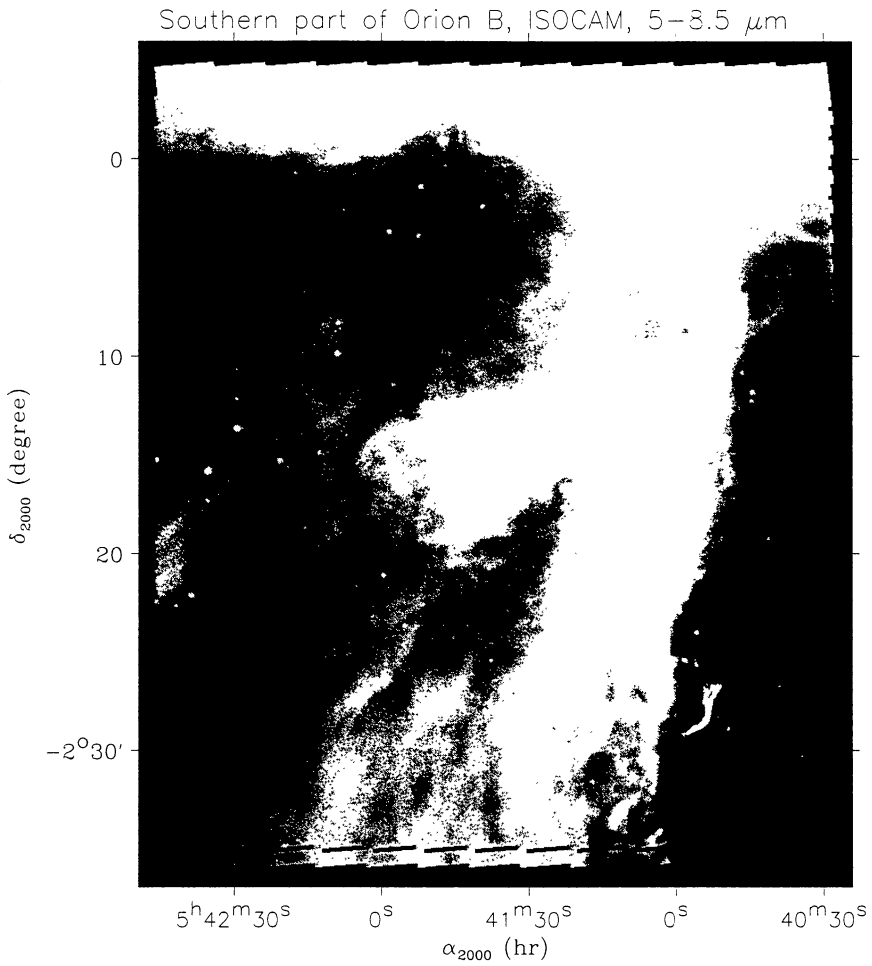

Figure 4. ISOCAM map of the Southern part of Orion B with the LW2 filter (5-8.5 μm). The contrast is so high that the bright structures in the reflection nebula NGC2023 in the central part and in the southern part of NGC 2024 to the north are not visible because of the limited grey scale.

illuminated by this star. The zone of interaction between radiation and dust is narrow, as suggested by the width of bright filaments in the region around $\alpha_{2000} \sim$ 16h26m, $\delta_{2000} \sim$ -24°22' (Figures 1 and 2). These filaments closely follow the western edge of the molecular cloud (Wilking & Lada 1976, Loren 1989). They do not necessarily correspond to filaments of dust, but to the illuminated edge of a dense cloud. The long axis of the filament appears on the ISOCAM image perpendicular to the projected star direction (Figure 2), confirming that the star is in this region the main heating source and at the center of a more or less spherical cavity. The filaments present interlaced structures likely due to an irregular shape of the edge of this cavity.

The brightness gradients across the filaments and along the projected direction of the star (Figure 3) are quite steep (within less than 1 arcmin or 0.05 pc). Most of the emission within the two filters LW2 and LW3 is due to emission features of aromatic hydrocarbons whose intensity globally scales with the UV radiation field (Boulanger et al. 1997). Therefore, at a first order, we can consider that the ISOCAM brightness is proportional to the column density of the emitting particles and the UV radiation field. IRAS data have shown that several dense clouds present a 12 μm limb–brightening effect at the edge with typical sizes of a few 10 arcmin, which may be due to an enhanced abundance of emitters (e.g. Bernard et al. 1993). However the width of the filament revealed by ISOCAM is ∼1 arcmin, so we assume that the relative abundance of the emitters is constant. Starting from the star, the brightness increase is essentially due to a positive density gradient, while the brightness decrease in the direction opposite to the star is due to the extinction of incident UV radiation emitted by the star.

The peak emission I_0 can be written: $I_0 = \epsilon\ \eta\ N_H\ \phi_0$, where ϵ is the emissivity of the emitting particles, η their relative abundance and N_H the col-

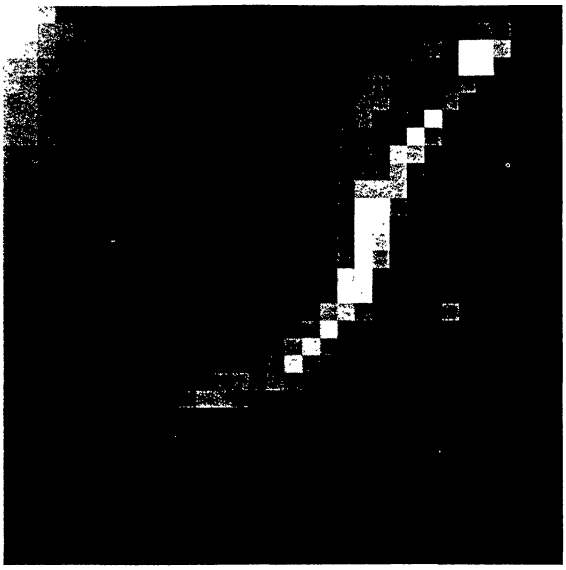

Figure 5. 32×32 image taken by ISOCAM with the LW2 filter of the edge of the Horsehead. This image has not been projected to avoid smoothing effects. North is up.

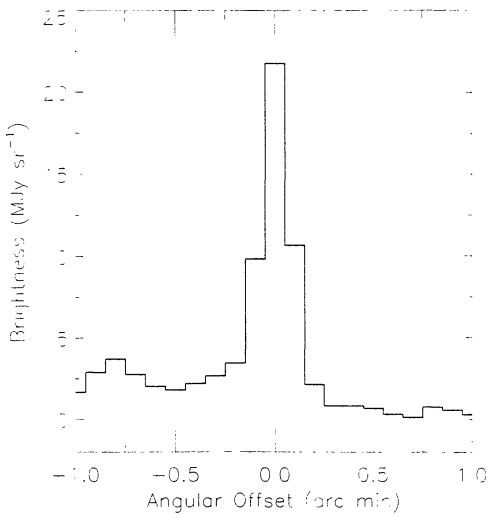

Figure 6. Horizontal profile (for the LW2 filter) along the brightest pixel at the edge of the Horsehead.

umn density. We assume that within the interface ϵ, η and N_H are constant. Adjusted with the law $I(z) = I_0\ e^{-Kz}$, the brightness decrease appears compatible with an extinction K= ∼1.8 arcmin^{-1}, corresponding to ∼38 pc^{-1} at a distance of 160 pc. If we assume that the medium is homogeneous and using standard conversion numbers (with τ_V/A_V= 1/1.096, A_V/N_H=1/1.9 10^{21} cm^{-2}, and τ_{UV}/τ_V= 2.8 from Roberge et al. 1981, we have: K= n × 4 10^{-3} pc^{-1}, n being the local density in units of cm^{-3}), we obtain a local density of ∼10^4 cm^{-3}. This a lower limit since the observed gradients should be smaller than local gradients because of projection effects (the real shape of the interface is unknown). However it is remarkable to notice that the $C^{18}O$ emission at the western edge of the ridge (∼ 2 K km s^{-1}, Wilking & Lada 1976) which closely follows the bright filaments also imply a local density of a few 10^4 cm^{-3}.

3.2. The PDR of the Horsehead in Orion B

ISOCAM observations reveal with the angular resolution of 6 arcsec the spatial structure of the southern part of Orion B (Figure 4 from Abergel et al. in prep). The measured emerging intensities of the CO (Kramer et al. 1996) and 158 μm C^+ lines (Jaffe et al. 1981) have indicated that the emissions arise from the surface of small clouds throughout the complex, and not only from a single layer at the edge. Except at the edges, most of the structures detected by ISOCAM are due to random superposition of individual clouds on the line of sights. Therefore the preliminary analysis we present in this paper concerns the Horsehead nebula, at the western edge of the complex (Abergel et al., in prep).

The Horsehead nebula is a dark cloud emerging from its parental complex L1630 due to UV eroding radiation emitted by the OB-systems ζ Ori to the north and σ Ori to the west (Reipurth & Bouchet 1984). Both systems are located at a projected distance of 0.5°, corresponding to ∼ 4 pc on the sky for a distance of 400 pc. However, Malin 1987 suggests that the ζ Ori system does not participate to the heating of the complex since it is located in the foreground, which is also confirmed by Hipparcos. The illuminated side of the Horsehead presents the sharpest IR filament detected in our Galaxy by ISOCAM (Figures 4 and 5), elongated toward the north-south direction. It is marginally resolve by ISOCAM, the FWHM being of the same order as the pixel size (6 arcsec). At a distance of 400 pc, 10 arcsec corresponds to ∼0.02 pc. The configuration is similar to the one revealed at the interface of ρ Oph, but the geometry is more simple: we only see an illuminated wall of matter, while for ρ Oph the interface appear more or less spherical. The increase of the emission on the illuminated side is due to an extremely steep increase of the column density, while the decrease on the east side is mainly due to extinction of the UV radiation emitted by σ Ori.

We use the same simple model as for ρ Oph. The illuminated edge is considered as a layer illuminated exactly edge-on. The decrease of the brightness toward the filament is compatible with an extinction coefficient K= 10 arcmin^{-1} (Figure 6), corresponding to ∼80 pc^{-1} at a distance of 400 pc. This is a lower limit, because of the dilution within the pixel field of view (the Point Spread Function is under-sampled for these observations). Using the relationship: K= n × 4 10^{-3} pc^{-1}, n being the local density assumed constant within the nebula (units: cm^{-3}), we obtain n= 2 10^4 cm^{-3}. Molecular observations (e.g. Kramer et al. 1996) have suggested that the average density in the nebula is within the range 1-3 10^4 cm^{-3}. We have assumed an infinite gradient at the illuminated edge which is unrealistic, as the simple modelisation

by an unique layer. However a lower density gradient and/or a more complex geometry would produce smoother brightness profiles because of projection effects.
These observations also allow to constrain the clumpiness of the material. For the same value of the average density, the UV radiation penetrates further in regions in which the material is clumped than in homogenous regions (Boissé 1990). Using the radiative transfer formalism developed by Boissé (1990) for two-phase clumpy regions, preliminary results (Abergel et al. in prep.) show that, at the edge of the Horsehead, the density contrasts between clumps and interclumps is strongly limited (typically lower than ~ 5).

3.3. Conclusion: Density structure of the interfaces

For the interfaces of ρ Oph and the Horsehead nebula, we reach the same conclusion. The brightness decrease can be explained by UV extinction within an homogeneous medium with a constant density derived from molecular observations, or a medium with limited density fluctuations at small scales (typically below 0.01 pc). Such a result may contradict the detection of very small molecular structures in several nearby clouds (e.g. Falgarone et al. 1998). However, the small scale density structure of the interfaces may be modified because of the strong illumination. Dense matter can be accumulated ahead of a shock (Loren & Wootten 1986) as suggested in ρ Oph by the coherence of the polarisation angle of IR absorption in this area (Vrba et al. 1976). The detection with ISOCAM of an extremely steep positive density gradient at the illuminated edge of the Horsehead supports this hypothesis.

4. DENSE CORES

In the theory of star formation, the dense starless cores are believed to be stellar progenitors. Opaque in the visible, they have been observed with different molecular lines such as NH_3, CS, $C^{18}O$, C_3H_2, DCO^+, HCO^+, or $H^{13}CO^+$ (e.g. Benson & Myers 1989, Butner et al. 1995). These observations give estimates of the central column density with assumptions about excitation and chemistry effects. However nothing was known about their density structure because of the limited angular resolution (at least a few 10"). Recent submillimeter and millimeter observations allow to detect the continuum emission emitted by dense cores (for instance at IRAM with an angular resolution of 11 arcsec, André et al. 1996, Motte et al. 1998). Assuming a constant dust temperature and a constant dust opacity in the core, the radial emission profiles appear consistent with a power law density $n(r) \propto r^{-2}$ in the outer regions. At radii less than a few thousands AU, the profiles systematically flatten out near the center. None of the profiles appear consistent with a singular r^{-2} isothermal sphere (Shu 1977). However, the cores are heated from the outside and the physical properties of the dust likely vary within the cores, therefore the two assumptions (constant temperature and constant opacity) are questionable.

Several dense cores have been revealed by ISOCAM in the main cloud of ρ Ophiuchi as sharp and deep absorption structures against the diffuse background (Abergel et al. 1996). Several absorption features have also been found by ISOCAM in the galactic plane (Omont, in these proceedings) a nd in a survey of selected dense cores (Bacmann et al., these proceedings). In order to derive mass estimates and density profiles from absorption measurements, it is necessary to estimate as properly as possible the background and foreground emissions, and the local density outside of the core. For one core in ρ Oph (Oph D), we have shown in Abergel et al. 1997 that the total mass derived from ISOCAM measurements (typically 5-10 $M_\odot$) is in good agreement with measurements deduced from DCO^+ and 1.3 mm observations. This agreement is obtained for the two filters (5-8.5 and 12-18 μm) using the infra-red extinction law of Draine & Lee (1984). We have also confirmed the central flattening of the internal regions (typically for $r < 0.02$ pc). The external parts of the steepest brightness gradient are compatible with r^{-2} or r^{-3} profiles, depending on the assumed external density (in a range constrained by molecular observations). It is actually difficult to give any definitive conclusions, since the real shape of the core is not known.

5. POWER SPECTRUM OF THE ISM AT SMALL SCALES

Images of the ISM appear self-similar over a very wide range of scales and densities. The relationship between the apparent fragmentation at different scale can be quantified by computing the spectral index of the power spectrum of the emission. Gautier et al. (1992) have found a power spectrum $P(k) \propto k^{-3}$ (k being the spatial frequency) for the IRAS emission at 100 μm, for angular scales going from a few degrees down to the angular resolution of IRAS, ~ 4 arcmin. For larger scales, the same power law has recently been obtained by Wright 1998 from the DIRBE data of the COBE satellite (at 100, 140 and 240 μm). Obviously, ISOCAM does not allow to observe the emission of the large grains component of the ISM which dominate the emission at these wavelengths. However, these grains are responsible of the infra-red extinction. ISOCAM observations of the main cloud of ρ Ophiuchi reveal a lot of structures seen in extinction, since it is illuminated on large scales from its far side by the Sco OB2 association (de Geus et al. 1989). Several dense cores are detected (see the previous section), but there are also absorption structures with a lower contrast which absorb the background emission, especially in the north-east part of the complex (Figure 1). In this region, likely most of the spatial fluctuations detected in the ISOCAM maps are due to extinction. This idea is also supported by the remarkable anti-correlation found between the ^{13}CO and the ISOCAM emissions. We have built power spectra of this region, and preliminary results for angular scales going from $\sim 0.1°$ down to ~ 6 arcsec indicates a k^{-3} law (Figure 7). By combining COBE, IRAS and ISOCAM data, we can conclude that the interstellar medium seems self-similar in diffuse regions for a range of angular scales going from several 10° down to a few arcsec.

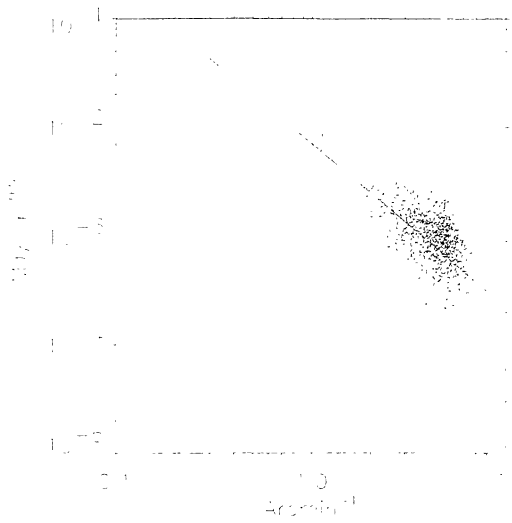

Figure 7. The square root of the two-dimensional power spectrum of the ISOCAM emission measured with the LW2 filter (5-8.5 μm). The solid line has a slope of -1.5, corresponding to a slope of -3 in the power spectrum.

6. CONCLUSIONS

The ISOCAM survey of different star forming regions has allowed to distangle between the contribution of embedded sources and extended emission. Individual structures can be analysed with an angular resolution of 3-6 arcsec.

The illuminated edges of the ρ Ophiuchi main cloud and of the Horsehead nebula presents bright and narrow filaments due to the interaction of incident radiation with the matter. These filaments can be explained by (1) steep density gradients at the interface and (2) the extinction of UV radiation within the dense clouds which appear homogeneous at small scales (typically lower than $\sim$ 0.01 pc for the Horsehead).

The spatial distribution of the column density of dense cores is revealed with unprecedented angular resolution and sensitivity. The density profiles depart from a r^{-2} law due to a central flattening of the internal regions (typically for $r < 0.02$ pc). The steepest gradients of extinction in outer regions can be modelled with a density profile at least as seep as a r^{-2} law.

The statistical analysis of the spatial distribution of dust in the interstellar medium is extended to angular scales unreachable before ISO (down to $\sim$ 6 arcsec). Preliminary results show that the interstellar medium seems self-similar in diffuse regions for a range of angular scales going from several 10° down to a few arcsec.

REFERENCES

Abergel A. et al. 1997, ASP 132, 220

Abergel A. et al. 1996, A&A, 315, L329

Abergel A. et al., 1998, Exp. Astron., in press

André P., et al. 1996, A&A 314, 625

Benson P.J., Myers P.C. 1989, ApJS 71, 89

Bernard. J.P., et al. 1993, A&A 277, 609

Bertiau F.C., 1958, ApJ 128, 533

Biviano, A., 1998 ESA report in prep.

Boisse 1990, A&A 228, 483

Boulanger. F., et al. 1990, ApJ, 364, 136

Boulanger F. et al. 1997, ASP, 132, 15

Butner H.M., et al. 1995, ApJ 448, 207

Cesarsky, C.J. et al., 1996, A&A 315, L32

de Geus E.J., et al. 1989, A&A 216, 44

Désert F. X., et al. 1990, A&A 237, 215

Désert F. X., et al. 1998, A&A, in press

Diamond, P.J., et al. 1989, ApJ, 347, 302

Draine B.T., Lee H.M., 1984, ApJ 285, 89

Dwek, E. et al. 1997, ApJ 475, 565

Falgarone, E. et al. 1998, A&A, 331, 669

Gautier III, T.N., et al. 1992, AJ, 103 (4), 1313

Giard, M., et al. 1994, A&A, 291, 239

Jaffe, D. et al. 1994, ApJ 436, 203

Kramer C., et al. 1996, A&A 307, 915

Léger, A., Puget, J.L. 1984, A&A, 137, L5

Loren R.B., 1989, ApJ 338, 902

Loren R.B., Wootten A., 1986, ApJ 306, 142

Malin, D., 1987, Sky & Telescope, 74, 253

Marscher. A.P., et al. 1993, ApJ 419, L101

Mattila, K. et al., 1996, A&A, 315, L353

Miville-Deschênes, M.-A. et al., 1999, in prep.

Motte, F. et al. 1998, A&A 336, 150

Moutou, C. et al. 1997, ASP, 132, 47

Reach W.T et al. 1995, Unveiling the cosmic infrared background. AIP press, New York, p. 37

Roberge, W.G et al. 1981, ApJ, 243, 817

Reipurth B., Bouchet P., 1984, A&A 137, L1

Sellgren, C. et al. 1985, ApJ 299, 416

Shu F. 1977, ApJ 214, 488

Vrba F.J., Strom S.E., Strom K.M., 1976, AJ 81, 958

Wilking B.A., Lada C.J., 1983, ApJ 274, 698

Wright, E.L. 1998, 496, 1